

27 Abstract

28 Dust is an important aerosol affecting air quality in China in winter and spring
29 ~~that~~seasons. Dust in China is potentially influenced by the interannual climate
30 variability associated with El Niño. Here, the impacts of El Niño with different temporal
31 and spatial types on dust pollution in boreal winter and spring in China and the potential
32 mechanisms are investigated using ~~ana~~ state-of-the-art earth system model (E3SMv1).
33 We find that the Eastern Pacific (EP) and Central Pacific (CP) El Niño both increase
34 wintertime dust concentrations by 5–50 $\mu\text{g m}^{-3}$ over central-eastern China. Due to a
35 stronger wind and lower relative humidity, which favor dust emissions near sources,
36 and a strengthened northwesterly and reduced precipitation, which are conducive to
37 dust transport, dust concentrations during the CP El Niño are 5–20 $\mu\text{g m}^{-3}$ higher in
38 northern China than during the EP El Niño, although the changes are mostly
39 insignificant. El Niño with a short duration (SD) increases boreal winter dust
40 concentrations by 20–100 $\mu\text{g m}^{-3}$ over northern China relative to the climatological
41 mean, while there is a decrease of 5–50 $\mu\text{g m}^{-3}$ during the long duration (LD) El Niño,
42 which are also related to the El Niño-induced changes in atmospheric circulation,
43 precipitation, and relative humidity. In the following spring season, all types of El Niño
44 events enhance dust over the northern China, but only the increase during the LD El
45 Niño is statistically significant, suggesting that the weaker intensity but longer duration
46 of the LD El Niño events can significantly affect spring dust in China. Our results
47 contribute the current knowledge of the influence of El Niño on dust pollution, which
48 have profound implications for air pollution control and dust storm prediction.

49 **1. Introduction**

50 Dust, one of the most important types of natural aerosols, has significant impacts
51 on Earth's radiative balance (Seinfeld et al., 2004), regional and global climate (Kok et
52 al, 2018; Yang et al.,2017), the hydrological cycle (Huang et al., 2014), agricultural
53 production (Sivakumar, 2005), public health and transportation activities (Goudie,
54 2014). The Gobi Desert and the Taklamakan Desert in northwestern China are
55 important contributors to dust concentrations in East Asia and even globally, and about
56 30% of the dust from the sources in China can be transported to the downwind areas
57 over long distances (Chen et al., 2017). Despite China's vigorous efforts to combat
58 desertification since the beginning of 21st century, strong and widespread dust storms
59 still occurred in China in recent years (Yin et al., 2021). Therefore, a deeper and more
60 scientific comprehension of the factors affecting dust aerosols in China is urgently
61 needed for the early warning and mitigation of dust pollution.

62 In recent years, the influence of meteorological conditions on dust pollution in
63 China has attracted considerable attention (Guo et al., 2019; Li et al., 2020; Lou et al.,
64 2016; Shi et al., 2021; Yin et al., 2021; Zhu et al., 2008). Under global warming in
65 recent decades, dust emissions and the frequency of dust storms in northern China
66 decreased (Shi et al., 2021), which was attributed to the reduced frequency and intensity
67 of Mongolian cyclones, related to the weakened westerly jet stream and atmospheric
68 pressure in northern China and Mongolia, in a warming climate (Zhu et al., 2008). Due
69 to a combination of changes in disruptive temperature anomalies in the Mongolian dust
70 source region, the occurrence of super Mongolian cyclone, and the anomalies of sea ice
71 in the Barents and Kara Sea and sea surface temperature (SST) in the east Pacific and
72 northwest Atlantic, China experienced the strongest dust pollution in spring 2021(Yin
73 et al., 2021). Lou et al. (2016) pointed out that springtime dust concentrations exhibited
74 a significant negative correlation with the East Asian Monsoon Index over most of
75 China with a correlation coefficient of -0.64 in their model simulations, and they found
76 that anomalous northwesterly winds in weak East Asian monsoon years led to a strong
77 dust transport from Mongolia to China. Mao et al. (2011) illustrated that the negative
78 (positive) phase of Arctic Oscillation (AO) can lead to an increase (decrease) in the
79 frequency of dust storms in northern China due to the increase (decrease) in the
80 frequency of cold air outbreak over Mongolia.

81 El Niño-Southern Oscillation (ENSO) is a well-known mode of climate variability

82 generated by coupled ocean-atmosphere interactions that can exert a far-reaching
83 impact on global climate despite its origin in the tropical Pacific Ocean (Trenberth,
84 1997; Yang et al., 2016a, 2016b; Zeng et al., 2021). Numerous studies have
85 demonstrated that El Niño can affect dust emission, concentration and transport by
86 modulating large-scale atmospheric circulation, precipitation and temperature (Le and
87 Bae, 2022; Lee et al., 2015; Li et al., 2021). Using observational data over 1961–2002,
88 Lee et al. (2015) found that ~~the~~ under the negative AO phase, frequency of spring dust
89 events in northern China during El Niño was 30% higher than that during La Niña years.
90 Li et al. (2021) used dust surface concentration data (1982–2019) from MERRA-2
91 reanalysis to study the impacts of ENSO events on global atmospheric dust loading and
92 found that dust concentrations were positively correlated with Southern Oscillation
93 Index (SOI, a consistently negative SOI is El Niño and the opposite is La Niña) over
94 northwestern China, which suggests that El Niño was associated with a decrease in dust
95 concentrations. Modeling studies driven by reanalysis data also revealed a relatively
96 weak positive relationship between SOI and dust emissions over Gobi Desert, although
97 this correlation has a large spatiotemporal variation (Gong et al., 2006; Hara et al., 2006).
98 These numerical studies used regional models driven by or nudged to reanalysis
99 meteorological fields, which could be influenced by factors other than El Niño. Recent
100 studies have indicated that the El Niño impact on air pollutants can be better represented
101 by the superposed SST perturbation method (Yu et al., 2019; Zhao et al., 2018; Zeng et
102 al., 2021), considering the influence of ENSO alone. To the best of our knowledge, no
103 study has yet used this approach to investigate the relationship between El Niño and
104 dust pollution in China.

105 Additionally, previous studies mainly focused on the influences of general El Niño
106 on dust over China, while El Niño can be classified into different temporal types (e.g.,
107 short duration (SD) and long duration (LD) El Niño; Guo and Tan, 2018) and spatial
108 types (e.g., East Pacific (EP) and Central Pacific (CP) El Niño; Kao and Yu, 2009).
109 During different spatial and temporal types of El Niño, patterns of precipitation and
110 atmospheric circulation are also different in China (Yu et al., 2019; Zeng et al., 2021),
111 and they could have distinct effects on wintertime and springtime dust pollution in
112 China. Nevertheless, most of the existing studies have focused on the effects of various
113 spatial and temporal types of El Niño events on anthropogenic aerosols, while few
114 studies have examined their effects on natural aerosols, such as dust, and their
115 associated mechanisms, which are crucial for predicting and combating dust pollution

116 in the near future.

117 In this work, the effects of different spatial and temporal types of El Niño on
118 wintertimeboreal winter and springtimespring dust pollution in China and the
119 mechanisms behind the impacts are examined using the Energy Exascale Earth System
120 Model version 1 (E3SMv1). The methods and model description are described in
121 Section 2. The quantitative impacts of various temporal and spatial types of El Niño
122 events on wintertime and springtime dust concentrations in China and the associated
123 mechanisms are elaborated in Section 3. Section 4 summarizes the key results and
124 conclusions of the study.

125

126 **2. Data and Methods**

127 **2.1 Data**

128 Global SST patterns and SST anomalies during El Niño events of different
129 temporal and spatial types are constructed using the merged Hadley-NOAA/OI dataset
130 which has a horizontal resolution of $1^\circ \times 1^\circ$ from 1870 to 2017 (Hurrell et al., 2008).
131 The monthly ERA5 reanalysis data (Hersbach et al., 2020) are applied to evaluate the
132 simulated meteorological parameters during El Niño events.

133 Hourly observations of PM₁₀ (particulate matter less than 10 μm in diameter)
134 concentrations in China from 2015 to 2021 derived from the China National
135 Environmental onitoring Centre (CNEMC) and the Deep Blue aerosol products
136 (Platnick et al., 2015) from Moderate Resolution Imaging Spectroradiometer (MODIS)
137 on Terra satellite, including monthly Aerosol Optical Depth (AOD) at 550 nm and the
138 Ångström exponent (α) from 2001–2020, are applied to evaluate the performance of
139 dust simulation in the model. The satellite dust optical depth (DOD) is calculated
140 following Yu et al. (2021).

141 **2.2 El Niño events identified as different spatial and temporal types**

142 We first clarify the definition of different temporal and spatial types of El Niño
143 events here. The notation of year⁰ is used to denote the first year of El Niño
144 development, and Jan⁰, Feb⁰, ..., and Dec⁰ indicate the individual months of that year,
145 while year^{1,2,...} and Jan^{1,2,...}, Feb^{1,2,...}, ..., and Dec^{1,2,...}, respectively, denote the
146 following years and months therein. Niño 3.4 index is defined as the anomalyarea-mean
147 anomalies of detrended SST in the Niño 3.4 region (170°W–120°W, 5°S–5°N). Niño
148 3/4 index ($I_{\text{Niño}3}/I_{\text{Niño}4}$) is same as Niño 3.4 index, but in the Niño 3/4 region (150°W–

149 90°W, 5°S–5°N; 160°E–150°W, 5°S–5°N).

150 For the classification of different temporal types, following Wu et al. (2019), El
151 Niño events are firstly selected if any of 3-month running averaged Niño 3.4 index
152 during Oct⁰–Feb¹ greater than 0.75°C. Then the LD El Niño event is identified once
153 any of Niño 3.4 index during Oct¹–Feb² is higher than 0.5°C; otherwise, it is a SD El
154 Niño event.

155 Following Yu et al. (2019), the El Niño events, selected with 3-month running
156 averaged Niño 3.4 indices higher than 0.5°C for five consecutive months, are classified
157 into different spatial types based on the EP El Niño index (I_{EP}) and the CP El Niño index
158 (I_{CP}). The definition of these indices is given below.

$$159 \quad I_{EP} = I_{Niño3} - \alpha \times I_{Niño4} \quad (1)$$

$$160 \quad I_{CP} = I_{Niño4} - \alpha \times I_{Niño3} \quad (2)$$

$$161 \quad \alpha = \begin{cases} 0.4, & I_{Niño3} \times I_{Niño4} > 0 \\ 0, & I_{Niño3} \times I_{Niño4} \leq 0 \end{cases} \quad (3)$$

162 If the mean I_{EP} is greater than the I_{CP} during Oct⁰–Feb¹ of an El Niño, then it is an
163 EP El Niño event; else, it is a CP El Niño event. Note that there also exist mixed El
164 Niño events that are not considered separately in this study.

165 The time series of Niño 3.4 index derived from Hadley-NOAA/OI 1870–2017 data
166 is shown in Figure S1. Using the definitions described above, for El Niño with different
167 temporal types, 22 SD El Niño events and 8 LD ones are extracted during this time
168 period; for El Niño with different spatial types, 26 EP El Niño events and 8 CP ones are
169 extracted. The mechanisms leading to different types of El Niño are given in Text S1.

170 **2.3 Model description and experimental design**

171 To investigate the impacts of El Niño of different spatial and temporal types on
172 dust aerosol in China, this study utilizes the U.S. Department of Energy (DOE)
173 E3SMv1 (Golaz et al., 2019). As a model developed from the well-known CESM1
174 (Community Earth System Model version 1), E3SMv1 provides significant
175 improvements to the atmospheric component, including processes associated with
176 aerosol, cloud, turbulence, and chemistry (Rasch et al., 2019). We choose the horizontal
177 resolution of about 1° and 30 vertical layers. E3SMv1 predicts aerosols including
178 mineral dust, sea salt, sulfate, primary and secondary organic aerosols, and black carbon
179 in the four-mode Modal Aerosol Module (MAM4) (Wang et al., 2020). E3SMv1
180 represents dust-related processes in the atmosphere and land model components (Feng
181 et al., 2022). Dust emissions are calculated at each model time step according to the

182 wind erosion dust scheme proposed by Zender et al. (2003), which is related to 10-
183 meter wind speed, surface soil moisture content, soil erodibility, vegetation cover and
184 threshold friction velocity.

185 The following simulations are performed. A “CLIM” experiment applying the
186 prescribed climatological mean of monthly SST during 1870–2017 is integrated for 30
187 years. Four sets of sensitivity simulations, “SD”, “LD”, “EP” and “CP”, are driven by
188 the monthly SST representing the composite of SD, LD, EP and CP El Niño events,
189 respectively, which is generated through adding the mean monthly SST anomalies from
190 Jul⁰ to Jun¹ of the SD, LD, EP, and CP El Niño events (Fig. S1), respectively, to the
191 climatological SST between 60°S and 60°N. All the sensitivity experiments have 3
192 ensemble members with diverse initial conditions branched from different years of the
193 CLIM simulation- and the results are based on the ensemble mean. All sensitivity
194 experiments are run for 13 years with the first 3 years as model spin-up and the last 10
195 years used for analysis. The differences of model fields between the sensitivity
196 simulations and CLIM represent the influences of El Niño events with different spatial
197 and temporal types on dust aerosols. All other external factors such as greenhouse gas
198 concentrations, insolation, anthropogenic aerosols and their precursor emissions are
199 hold at present-day conditions (year 2014). The SST anomalies relative to the 1870–
200 2017 climatology during SD, LD, EP and CP El Niño events are shown in Fig. 1.

201 **2.34 Model evaluation**

202 To evaluate the model performance in dust simulation, we compare the simulated
203 near-surface dust concentration and dust optical depth (DOD) over China with observed
204 PM₁₀ concentrations and satellite retrieved DOD, respectively. The model can
205 reproduce the spatial distribution of springtime dust in China, with high dust
206 concentrations in northwestern China and low in southern and northeastern China (Fig.
207 S2). The spatial correlation coefficient between the simulated dust concentrations in
208 E3SMv1 and observed near-surface PM₁₀ concentrations is +0.55. However, the model
209 strongly overestimates dust concentrations over the source regions, which were also
210 reported in many previous studies using the E3SMv1 and CESM (the predecessor of
211 E3SMv1) (Wang et al., 2020; Wu et al., 2019). The high model bias near the sources is
212 also confirmed by comparing DOD between model simulation and satellite retrieval. It
213 suggests that the dust emissions are overestimated in northwestern China in the model.

214 The high bias is partly related to the dust treatment in the model that dust is emitted
215 into a shallow model bottom layer in E3SMv1 for increased model vertical resolution

216 (Wang et al., 2020). In addition, stronger 10-m wind speed simulated by the model
217 compared to the observation (Fig. S3) also contributes to the higher dust loading.

218 However, we also note that the E3SMv1 underestimates the transport of dust from
219 source regions (Wu et al., 2020; Feng et al., 2022), thus the dust over eastern China is
220 comparable to observations.

221 **3. Results**

222 **3.1 Impacts of different El Niño types on winter dust pollution**

223 The simulated effects of the four types of El Niño with different spatial positions
224 (EP and CP) and durations (SD and LD) on the DJF ground-level dust concentrations
225 are shown in Fig. 2. As for different spatial types of El Niño events, the effects on DJF
226 dust concentrations in China are similar, with an increase in dust concentrations of 5–
227 50 $\mu\text{g m}^{-3}$ over central-eastern China during EP and CP El Niño compared to the
228 climatological means. The spatial pattern of dust changes is consistent with previous
229 modeling studies (Lee et al., 2015; Li et al., 2021). Although the influences of EP and
230 CP El Niño on the DJF dust concentrations resemble each other in the spatial patterns
231 over China, the magnitudes of the influences are different. During CP El Niño relative
232 to the climatological mean, dust concentrations increase more significantly over
233 central-eastern China, with the increases of 20–50 $\mu\text{g m}^{-3}$, 5–20 $\mu\text{g m}^{-3}$ higher than that
234 during EP El Niño. relative to the climatological mean. The large increase during CP El
235 Niño relative to the climatological mean is also more widespread than that during EP
236 El Niño relative to the climatological mean. Compared to CP El Niño, dust
237 concentration over central-eastern China decreased slightly during the EP El Niño, but
238 the changes are mostly insignificant.

239 As for different temporal types of El Niño events, their effects on DJF dust
240 concentrations over China are quite different. SD El Niño events cause an increase in
241 DJF near-surface dust concentrations of 20–100 $\mu\text{g m}^{-3}$ in northern China and about 5–
242 20 $\mu\text{g m}^{-3}$ in southern China. Whereas during LD El Niño events, winter dust
243 concentrations have a decrease of about 5–50 $\mu\text{g m}^{-3}$ in northern and northeastern China
244 relative to the climatology and no significant change is shown in southern China. In
245 contrast to LD El Niño events, SD El Niño events have positive DJF dust concentration
246 anomalies of 5–20 $\mu\text{g m}^{-3}$ in southern China and a maximum over 100 $\mu\text{g m}^{-3}$ in
247 northern China and the Gobi Desert. Furthermore, DJF dust concentrations over the
248 Taklamakan Desert, one of the largest dust sources in China, have an increase during

249 LD El Niño events and an insignificant decrease during SD El Niño events.

250 Overall, these changes in dust concentrations indicate that CP El Niño events have
251 stronger and more widespread impacts on DJF dust concentrations than EP El Niño
252 relative to the climatological mean, and the SD and LD El Niño events exert opposite
253 impacts on DJF dust in China.

254 **3.2 Mechanisms of the different El Niño impacts on winter dust**

255 Meteorological factors such as 10-m wind speed, relative humidity and
256 atmospheric circulation play a dominant role in altering dust concentrations by altering
257 emissions, atmospheric transport, and wet scavenging of dust (Csavina et al., 2014).
258 Dust changes are also controlled by the El Niño-related changes in atmospheric
259 circulation and precipitation (Gong et al., 2006; Hara et al., 2006). The 10-m wind speed,
260 atmospheric circulation, relative humidity, precipitation anomalies, and related
261 processes during EP, CP, SD and LD El Niño are investigated here to reveal the
262 mechanisms of the influence of the four types of El Niño on dust over China.

263 During the CP, EP, and SD El Niño, DJF mean 10-m wind speed increases in the
264 Gobi Desert and northwestern China compared to the climatological mean (Fig. 3),
265 which favors the local dust emission over these regions. Whereas for the LD El Niño
266 event, the positive 10-m wind speed anomaly is greatly weakened, compared to the
267 other three types of El Niño events, and negative 10-m wind speed anomalies are
268 triggered in the Gobi Desert and northern China (Fig. 3e), which is not conducive to
269 dust emission during the LD El Niño events. The CP El Niño events trigger stronger
270 positive 10-m wind speed anomalies ($0.1\text{--}0.3\text{ m s}^{-1}$) than the EP El Niño events over
271 the Gobi Desert and northern China (Fig. 3c), which could lead to a greater local dust
272 emission. Compare to the LD El Niño, SD El Niño events produce significant positive
273 10-m wind speed anomalies of approximately 0.3 m s^{-1} in the Gobi Desert and northern
274 China (Fig. 3f), which is consistent with the increase/decrease in local DJF dust
275 concentrations during the SD/LD El Niño (Fig. 2). This suggests the importance of 10-
276 m wind speed in the dust changes during the El Niño events in China.

277 Figure 4 shows the atmospheric circulation anomalies for the four El Niño events.
278 All types of El Niño have negative anomalies of sea level pressure (SLP) in central-
279 eastern China, except the LD El Niño that shows a negligible SLP change in winter.
280 Meanwhile, during the EP, CP, and SD El Niño events, anomalous Mongolian cyclone
281 can strengthen the local ascending flow to lift more dust particles into the free
282 atmosphere. The anomalous northwesterly during CP and SD El Niño (Figs. 3b and 3d)

283 can transport these dust aerosols to central-eastern China, leading to the strong increases
284 in dust concentrations there (Figs. 2b and 2d). While during the LD El Niño, the lower
285 atmosphere in the Gobi Desert and northern China is controlled by a weak anomalous
286 high pressure accompanied by anomalous southeasterly that weakens the prevailing
287 northwesterly in winter and hinders the vertical lifting and southward transport of dust.

288 Our previous work has confirmed the ability of E3SM in reproducing the
289 atmospheric circulation in El Niño with different durations (Zeng et al, 2021). Here we
290 further evaluate the circulations in E3SM simulations during EP and CP El Niño events
291 by using ERA5 reanalysis data. The anomalous DJF mean 10-m wind speed and 850
292 hPa wind fields in the typical EP El Niño (2006/07) and CP El Niño (2014/15) relative
293 to the climatology (1950–2017) from ERA5 are presented in Fig. 5. Although the
294 increase in 10-m wind speed over northwestern China in the EP El Niño simulated in
295 the model is inconsistent with the ERA5 results, E3SM does capture the large increase
296 in wind speed over the Gobi Desert during the CP El Niño relative to the climatological
297 mean and EP El Niño. Moreover, the anomalies in wind fields during EP and CP El
298 Niño (i.e., anomalous southerly during EP El Niño and anomalous northwesterly during
299 CP El Niño) are well reproduced by E3SM. It suggests that the atmospheric circulation
300 features over central-eastern China during different types of El Niño are roughly
301 captured by the model. ~~Also~~ However, we note that ~~the observational~~ there are notably
302 differences in atmospheric circulation over many regions of East Asia. It can be partly
303 attributed to the model bias in reproducing the atmospheric responses to El Niño. The
304 observations can also be induced by other climate factors besides El Niño, leading to a
305 potential inconsistency in El Niño impact between model and observation.

306 The effect of relative humidity (RH) on dust concentration is also essential,
307 considering that a decrease in RH leads to a decrease in the threshold friction velocity
308 at high RHs (>40%), which further enhances dust emission flux and atmospheric
309 concentration (Csavina et al., 2014). Both EP and CP El Niño events have negative
310 anomalies in DJF RH in the Gobi Desert (Figs. 6a and 6b). The decrease in RH reduces
311 the dust threshold friction velocity and favors dust emission from the Gobi Desert. The
312 CP El Niño produces more pronounced and widespread negative RH anomalies in the
313 Gobi Desert and northwestern China than the EP El Niño. It gives approximately 3%
314 stronger negative RH anomalies (Fig. 6c), resulting in stronger and more widespread
315 increases in DJF dust concentrations during the CP El Niño event (Fig. 2c). As for El
316 Niño with different duration, the SD El Niño leads to significant decreases in DJF RH

317 of about 3% near the south part of the Gobi Desert, while increases in RH are located
318 over north part of the Gobi Desert during the LD El Niño (Figs. 6g and 6j), likely
319 resulting in the opposite changes in dust emissions. The ERA5 reanalysis data also
320 show the same RH variations during the different spatial and temporal types of El Niño
321 as the E3SM simulations described above (Fig. S3S4). Among all four types of El Niño
322 events, RH anomalies are consistent with the distribution of dust concentration
323 anomalies, which indicates that RH plays an important role in affecting variations in
324 dust emissions and concentrations in China during El Niño.

325 Fig. 7 shows the simulated changes in DJF dust emissions during different El Niño
326 events. During the EP and CP El Niño, DJF dust emissions are enhanced in the Gobi
327 Desert and northwestern China relative to the climatological average. The dust emission
328 increase is larger during the CP El Niño than the EP El Niño, which is consistent with
329 the higher positive DJF dust concentration anomalies during the CP El Niño.
330 Furthermore, the SD El Niño causes a significant increase in dust emissions of about
331 $0.5 \text{ g m}^{-2} \text{ d}^{-1}$ in the Gobi Desert compared to CLIM, while the LD El Niño causes a
332 decrease in dust emissions. These suggest that different types of El Niño events alter
333 the DJF dust emissions in China by changing the 10-m wind speed and RH, which is
334 the important cause of the variation in DJF dust concentrations in China.

335 Furthermore, a reduced DJF precipitation during both EP and CP El Niño events
336 ~~weakens(Fig. S5) should weaken~~ the wet removal of dust from the atmosphere in
337 northern China ~~(Fig. S4), further enhancing the~~. ~~However, only insignificant decreases~~
338 ~~in wet deposition appear in part of northern China and significant~~ increases in ~~DJF~~wet
339 ~~deposition are located in central and southern China related to increases in dust loading~~
340 ~~during EP and CP El Niño events (Fig. S6). It suggests that El Niño impact on~~ dust
341 concentrations ~~is mainly through changing the emission and transport of dust rather~~
342 ~~than the scavenging in winter~~.

343 3.3 Spring dust pollution affected by El Niño events

344 The changes in near-surface dust concentrations over China in the following spring
345 during the decaying phase for different spatial and temporal types of El Niño are also
346 examined (Fig. 8). During the following spring, all El Niño events trigger large positive
347 anomalies of March-April-May (MAM) dust concentrations in northern China.
348 However, the increases in dust concentrations during the EP, CP and SD El Niño relative
349 to the climatological average fail the 90% significance test, indicating that the effects
350 of these types of El Niño events on the dust pollution in northern China in the following

351 spring are uncertain, likely related to the large internal variability of the climate system.
352 In contrast to the strong reduction in dust concentrations over the Gobi Desert and
353 northern China during the LD El Niño in DJF, the effect in MAM reverses to a
354 significant increase in dust concentrations over these regions by 50–100 $\mu\text{g m}^{-3}$ (Fig.
355 8e). It suggests that the weaker intensity but longer duration of LD El Niño than the SD
356 El Niño can significantly affect spring dust aerosols in China.

357 During LD El Niño events, MAM 10-m wind speed significantly increases over
358 the Gobi Desert (Fig. S5S7), which facilitates the local dust emissions, although RH
359 only shows an insignificant decrease over the dust source region (Fig. S6S8). It can be
360 confirmed by the significant increases in MAM dust emissions by about 0.5 $\text{g m}^{-2} \text{d}^{-1}$
361 over the Gobi Desert and northwestern China during LD El Niño events (Fig. 9). Then
362 the strengthened northwesterly brings more dust to northern China during LD El Niño
363 events (Fig. S7S9). Along the transport pathway, the weakened precipitation (Fig. S10)
364 partly reduces the dust wet removal (Fig. S8S11), leading to the strong increase in
365 MAM dust concentration over northern China during the LD El Niño. However, this
366 effect is largely overwhelmed by the increased dust wet removal due to the emission-
367 induced increase in dust concentrations.

368

369 4. Conclusion and discussions

370 Dust, as an important air pollutant affecting air quality in China in winter and
371 spring, can be modulated by the interannual variations in El Niño-induced atmospheric
372 circulation and precipitation anomalies. In this study, the state-of-the-art E3SM model
373 is used to simulate the effects of different temporal types of El Niño events with short
374 (SD) and long duration (LD) and different spatial locations of El Niño events with sea
375 surface temperature anomalies located in Central Pacific (CP) and Eastern Pacific (EP)
376 on dust concentrations in China.

377 Both CP and EP El Niño events cause 5–50 $\mu\text{g m}^{-3}$ positive anomalies in winter
378 (DJF months) surface dust concentrations in central-eastern China. Compared to the EP
379 El Niño, the CP El Niño triggers a stronger wind and negative RH anomalies that lead
380 to greater local dust emissions. Then the anomalous northwesterly transports the dust
381 aerosols to central-eastern China during the CP El Niño, ~~accompanied by a reduced~~
382 ~~precipitation and wet removal of dust from the atmosphere,~~ resulting in 5–20 $\mu\text{g m}^{-3}$
383 higher and more widespread DJF dust concentration increases in northern China.

384 although the changes are mostly statistically insignificant. For the different temporal
385 types of El Niño events, wind speed significantly increases over the Gobi Desert and
386 northern China during the SD El Niño, favoring dust emissions. Meanwhile, the
387 anomalous northwesterly can increase the transport of dust aerosols to central-eastern
388 China, leading to an increase in DJF near-surface dust concentrations of 20–100 $\mu\text{g m}^{-3}$
389 ³ in northern China and 5–20 $\mu\text{g m}^{-3}$ in southern China relative to the climatological
390 mean. On the contrary, the LD El Niño reduces wind speed over the Gobi Desert and
391 northern China, which weakens dust emissions, accompanied with the atmospheric
392 circulation anomalies unfavorable for dust transport, leading to the DJF dust
393 concentration decrease by 5–50 $\mu\text{g m}^{-3}$ in northern and northeastern China relative to
394 the climatological mean.

395 In the following spring season, the four types of El Niño events with different
396 durations and spatial positions all cause positive dust concentration anomalies in
397 northern China. However, only the changes during the LD El Niño are statistically
398 significant. This is mainly due to an increase in 10-m wind speed over the Gobi Desert
399 during the LD El Niño, which enhances the local dust emissions, and then the
400 strengthened northwesterly brings more dust to the northern China. ~~At the same time,~~
401 ~~the weakened precipitation reduces the dust wet removal along the transport pathway.~~
402 It suggests that the weaker intensity but longer duration of LD El Niño events than SD
403 El Niño can significantly affect dust aerosols in China in spring.

404 In this study, the dust concentrations are evaluated by comparing modeled
405 concentrations with MAM PM₁₀ concentrations and the dust loading is also evaluated
406 by comparing modeled DOD with that derived from satellite data. However, the
407 anomalies of dust concentrations were not compared with observations. This is because
408 that dust is jointly influenced by many factors in the observation other than El Niño,
409 such as Mongolian cyclone, sea ice in the Barents Sea, sea surface temperature in
410 Atlantic Ocean, Arctic Oscillation, and human activities (Fan et al 2016, 2018; Mao et
411 al., 2011; Wang et al., 2021; Xiao et al., 2015; Yin et al., 2021), while this study presents
412 the “pure” effects of El Niño on dust using an Earth system model. In addition, PM₁₀ is
413 strongly influenced by other anthropogenic aerosols over eastern China, especially in
414 hazy winter. The comprehensive understanding of the impacts from different types of
415 El Niño events on dust in China requires a longer-term observation with sufficient
416 spatial coverage.

417 Our results contribute to the current knowledge of the vital influence of different

418 types of El Niño on dust pollution in winter and spring over China, which have
419 profound implications for air pollution control and dust storm prediction in China.
420 Notwithstanding, we also note that the E3SMv1 overestimates dust emissions from the
421 source regions and underestimates the long-range transport of dust (Wu et al., 2020;
422 Feng et al, 2022), ~~which may lead to biases in the estimate of El Niño impact on dust~~
423 ~~concentrations in China.~~ This high bias of dust loading near the dust source regions
424 are related to the dust treatment in the model, dust parameterization and stronger winds
425 in model than observations. The low bias of long-range transport of dust is due to the
426 strong dust deposition considering that dust is emitted in the shallow model bottom
427 layer in the model. Therefore, the estimate of El Niño impact on dust emissions and
428 concentrations are likely to be overestimated near the source regions, but impact from
429 changes in large-scale circulation related to El Niño on dust transport is possibly
430 underestimated. Also, results from a single model with relative short simulations may
431 not be representative and may not well remove the internal atmospheric variability,
432 which can be further investigated by conducting large ensemble and longer simulations
433 using multi-models. In future studies, the influences of different types of La Niña, the
434 cooling phase of ENSO, on dust pollution in China, warrants further investigation.
435 Besides, other natural aerosols, such as sea salt, are also influenced by El Niño events,
436 which is not taken into account in this study. In addition to natural sources, dust in
437 China can also be from anthropogenic emissions (Chen et al., 2019; Xia et al., 2022),
438 and their relations with El Niño require further study.
439

440 ***Code and data availability***

441 The E3SMv1 model is available at <https://github.com/E3SM-Project/E3SM> (last access:
442 25 Mar 2022) (<http://doi.org/10.11578/E3SM/dc.20180418.36>, E3SM project, 2018).

443 Our results can be made available upon request.

444

445 ***Author contributions***

446 YY designed the research and analyzed the data. LZ performed the model simulations.

447 All the authors including HW, PW, and HL discussed the results and wrote the paper.

448

449 ***Competing interests***

450 The authors declare that they have no conflict of interest.

451

452 ***Acknowledgments***

453 HW acknowledges the support by the U.S. Department of Energy (DOE), Office of
454 Science, Office of Biological and Environmental Research (BER), as part of the Earth
455 and Environmental System Modeling program. The Pacific Northwest National
456 Laboratory (PNNL) is operated for DOE by the Battelle Memorial Institute under
457 contract DE-AC05-76RLO1830.

458

459 ***Financial support***

460 This study was supported by the National Natural Science Foundation of China (grant
461 41975159), the National Key Research and Development Program of China (grant
462 2020YFA0607803 and 2019YFA0606800) and Jiangsu Science Fund for Distinguished
463 Young Scholars (grant BK20211541).

464 **References**

- 465 Chen S. Y., Huang J. P., Li J. X., Jia R., Jiang N. X., Kang L. T., Ma X. J., and Xie T.
466 T.: Comparison of dust emissions, transport, and deposition between the
467 Taklimakan Desert and Gobi Desert from 2007 to 2011. *Sci. China Earth Sci.*, 60,
468 1338–1355, <https://doi.org/10.1007/s11430-016-9051-0>, 2017.
- 469 Chen, S., Zhang, X., Lin, J., Huang, J., Zhao, D., Yuan, T., Huang, K., Luo, Y., Jia, Z.,
470 and Zang, Z.: Fugitive Road Dust PM_{2.5} Emissions and Their Potential Health
471 Impacts, *Environ. Sci. Technol.*, 53, 8455–8465,
472 <https://doi.org/10.1021/acs.est.9b00666>, 2019.
- 473 Csavina, J., Field, J., Felix, O., Corral-Avitia, A. Y., Saez, A. E., and Betterton, E. A.:
474 Effect of wind speed and relative humidity on atmospheric dust concentrations in
475 semi-arid climates, *Sci Total Environ*, 487, 82–90,
476 <https://doi.org/10.1016/j.scitotenv.2014.03.138>, 2014.
- 477 E3SM Project: Energy Exascale Earth System Model v1.0: Computer Software, DOE
478 [data set], <https://doi.org/10.11578/E3SM/dc.20180418.36>, 2018.
- 479 [Fan, K., Xie, Z., and Xu, Z.: Two different periods of high dust weather frequency in](#)
480 [northern China, *Atmos. Ocean. Sci. Lett.*, 9, 263–269,](#)
481 <https://doi.org/10.1080/16742834.2016.1176300>, 2016.
- 482 [Fan, K., Xie, Z., Wang, H., Xu, Z., and Liu, J.: Frequency of spring dust weather in](#)
483 [North China linked to sea ice variability in the Barents Sea, *Clim. Dyn.*, 51, 4439–](#)
484 [4450, https://doi.org/10.1007/s00382-016-3515-7](https://doi.org/10.1007/s00382-016-3515-7), 2018.
- 485 Feng, Y., Wang, H., Rasch, P. J., Zhang, K., Lin, W., Tang, Q., Xie, S., Hamilton, D. S.,
486 Mahowald, N., and Yu, H.: Global dust cycle and direct radiative effect in the
487 E3SM version 1: Impact of increasing model resolution, ~~*Earth and Space Science*~~
488 ~~*Open Archive*~~, <https://doi.org/10.1002/essoar.10510950.1>, in review for *J. Adv.*
489 *Model. Earth Sys.*, 14, e2021MS002909. <https://doi.org/10.1029/2021MS002909>,
490 2022.
- 491 Golaz, J. C., Caldwell, P. M., Van Roekel, L. P., Petersen, M. R., Tang, Q., Wolfe, J. D.,
492 Abeshu, G., Anantharaj, V., Asay - Davis, X. S., Bader, D. C., Baldwin, S. A.,
493 Bisht, G., Bogenschütz, P. A., Branstetter, M., Brunke, M. A., Brus, S. R., Burrows,
494 S. M., Cameron - Smith, P. J., Donahue, A. S., Deakin, M., Easter, R. C., Evans,
495 K. J., Feng, Y., Flanner, M., Foucar, J. G., Fyke, J. G., Griffin, B. M., Hannay, C.,
496 Harrop, B. E., Hoffman, M. J., Hunke, E. C., Jacob, R. L., Jacobsen, D. W., Jeffery,

497 N., Jones, P. W., Keen, N. D., Klein, S. A., Larson, V. E., Leung, L. R., Li, H. Y.,
498 Lin, W., Lipscomb, W. H., Ma, P. L., Mahajan, S., Maltrud, M. E., Mametjanov,
499 A., McClean, J. L., McCoy, R. B., Neale, R. B., Price, S. F., Qian, Y., Rasch, P. J.,
500 Reeves Eyre, J. E. J., Riley, W. J., Ringler, T. D., Roberts, A. F., Roesler, E. L.,
501 Salinger, A. G., Shaheen, Z., Shi, X., Singh, B., Tang, J., Taylor, M. A., Thornton,
502 P. E., Turner, A. K., Veneziani, M., Wan, H., Wang, H., Wang, S., Williams, D. N.,
503 Wolfram, P. J., Worley, P. H., Xie, S., Yang, Y., Yoon, J. H., Zelinka, M. D., Zender,
504 C. S., Zeng, X., Zhang, C., Zhang, K., Zhang, Y., Zheng, X., Zhou, T., and Zhu,
505 Q.: The DOE E3SM Coupled Model Version 1: Overview and Evaluation at
506 Standard Resolution, *J. Adv. Model. Earth Sys.*, 11, 2089–2129,
507 <https://doi.org/10.1029/2018MS001603>, 2019.

508 Gong, S. L., Zhang, X. Y., Zhao, T. L., Zhang, X. B., Barrie, L. A., McKendry, I. G.,
509 and Zhao, C. S.: A Simulated Climatology of Asian Dust Aerosol and Its Trans-
510 Pacific Transport. Part I: Interannual Variability and Climate, *J. Clim.*, 19, 104–
511 122, <https://doi.org/10.1175/JCLI3606.1>, 2006.

512 Goudie, A. S.: Desert dust and human health disorders, *Environ. Int.*, 63, 101–113,
513 <https://doi.org/10.1016/j.envint.2013.10.011>, 2014.

514 Guo, J., Xu, H., Liu, L., Chen, D., Peng, Y., Yim, S. H.-L., Yang, Y., Li, J., Zhao, C.,
515 and Zhai, P.: The trend reversal of dust aerosol over East Asia and the North Pacific
516 Ocean attributed to large-scale meteorology, deposition, and soil moisture. *J.*
517 *Geophys. Res. Atmos.*, 124, 10450–10466.
518 <https://doi.org/10.1029/2019JD030654>, 2019.

519 Guo, Y., and Tan, Z.: Westward migration of tropical cyclone rapid-intensification over
520 the Northwestern Pacific during short duration El Nino, *Nat. Commun.*, 9, 1507,
521 <https://doi.org/10.1038/s41467-018-03945-y>, 2018.

522 Hara, Y., Uno, I., and Wang, Z.: Long-term variation of Asian dust and related climate
523 factors, *Atmos. Environ.* 40, 6730–6740,
524 <https://doi.org/10.1016/j.atmosenv.2006.05.080>, 2006.

525 Hersbach, H., Bell, B., Berrisford, P., Hirahara, S., Horányi, A., Muñoz-Sabater, J.,
526 Nicolas, J., Peubey, C., Radu, R., Schepers, D., Simmons, A., Soci, C., Abdalla,
527 S., Abellan, X., Balsamo, G., Bechtold, P., Biavati, G., Bidlot, J., Bonavita, M.,
528 Chiara, G. D., Dahlgren, P., Dee, D., Diamantakis, M., Dragani, R., Flemming, J.,
529 Forbes, R., Fuentes, M., Geer, A., Haimberger, L., Healy, S., Hogan, R. J., Hólm,
530 E., Janisková, M., Keeley, S., Laloyaux, P., Lopez, P., Lupu, C., Radnoti, G.,

531 Rosnay, P. de, Rozum, I., Vamborg, F., Villaume, S., and Thépaut, J.-N.: The ERA5
532 Global Reanalysis, *Q. J. Roy. Meteor. Soc.*, 146, 1999–2049,
533 <https://doi.org/10.1002/qj.3803>, 2020.

534 Huang, J., Wang, T., Wang, W., Li, Z., and Yan, H.: Climate effects of dust aerosols
535 over East Asian arid and semiarid regions, *J. Geophys. Res. Atmos.*, 119, 11,398–
536 11,416, <https://doi.org/10.1002/2014JD021796>, 2014.

537 Hurrell, J. W., Hack, J. J., Shea, D., Caron, J. M., and Rosinski, J.: A new sea surface
538 temperature and sea ice boundary dataset for the Community Atmosphere Model,
539 *J. Clim.*, 21, 5145–5153, <https://doi.org/10.1175/2008jcli2292.1>, 2008.

540 Kao, H-Y., and Yu, J-Y.: Contrasting Eastern-Pacific and Central-Pacific Types of
541 ENSO, *J. Clim.*, 22, 615–632, <https://doi.org/10.1175/2008jcli2309.1>, 2009.

542 Kok, J. F., Ward, D. S., Mahowald, N. M., and Evan, A. T.: Global and regional
543 importance of the direct dust-climate feedback. *Nat. Commun.*, 9, 241,
544 <https://doi.org/10.1038/s41467-017-02620-y>, 2018.

545 [Le, T. and Bae, D.-H.: Causal influences of El Niño-Southern Oscillation on global dust](#)
546 [activities, *Atmos. Chem. Phys.*, 22, 5253-5263, \[https://doi.org/10.5194/acp-22-\]\(https://doi.org/10.5194/acp-22-5253-2022\)](#)
547 [5253-2022, 2022.](#)

548 Lee, Y. G., Kim, J., Ho, C.-H., An, S.-I., Cho, H.-K., Mao, R., Tian, B., Wu, D., Lee, J.
549 N., Kalashnikova, O., Choi, Y., and Yeh, S.-W.: The effects of ENSO under
550 negative AO phase on spring dust activity over northern China: an observational
551 investigation, *Int. J. Climatol.*, 35, 935–947, <https://doi.org/10.1002/joc.4028>,
552 2015.

553 Li, J., Garshick, E., Al-Hemoud, A., Huang, S., and Koutrakis, P.: Impacts of
554 meteorology and vegetation on surface dust concentrations in Middle Eastern
555 countries, *Sci. Total Environ.*, 712, 136597,
556 <https://doi.org/10.1016/j.scitotenv.2020.136597>, 2020.

557 Li, J., Garshick, E., Huang, S., and Koutrakis, P.: Impacts of El Niño-Southern
558 Oscillation on surface dust levels across the world during 1982–2019, *Sci. Total*
559 *Environ.*, 769, 144566, <https://doi.org/10.1016/j.scitotenv.2020.144566>, 2021.

560 Lou, S., Russell, L. M., Yang, Y., Xu, L., Lamjiri, M. A., DeFlorio, M. J., Miller, A. J.,
561 Ghan, S. J., Liu, Y., and Singh, B.: Impacts of the East Asian Monsoon on
562 springtime dust concentrations over China, *J. Geophys. Res. Atmos.*, 121, 8137–
563 8152, <https://doi.org/10.1002/2016JD024758>, 2016.

564 Mao, R., Gong, D., Bao, J., and Fan, Y.: Possible influence of Arctic Oscillation on dust

565 storm frequency in North China. *J. Geogr. Sci.* 21, 207–218,
566 <https://doi.org/10.1007/s11442-011-0839-4>, 2011.

567 Platnick, S., Hubanks, P., Meyer, K., and King, M. D.: MODIS Atmosphere L3 Monthly
568 Product (08_L3). NASA MODIS Adaptive Processing System, Goddard Space
569 Flight Center, http://dx.doi.org/10.5067/MODIS/MOD08_M3.006, 2015.

570 Rasch, P. J., Xie, S., Ma, P. L., Lin, W., Wang, H., Tang, Q., Burrows, S. M., Caldwell,
571 P., Zhang, K., Easter, R. C., Cameron-Smith, P., Singh, B., Wan, H., Golaz, J. C.,
572 Harrop, B. E., Roesler, E., Bacmeister, J., Larson, V. E., Evans, K. J., Qian, Y.,
573 Taylor, M., Leung, L. R., Zhang, Y., Brent, L., Branstetter, M., Hannay, C.,
574 Mahajan, S., Mamejtanov, A., Neale, R., Richter, J. H., Yoon, J. H., Zender, C. S.,
575 Bader, D., Flanner, M., Foucar, J. G., Jacob, R., Keen, N., Klein, S. A., Liu, X.,
576 Salinger, A. G., Shrivastava, M., and Yang, Y.: An Overview of the Atmospheric
577 Component of the Energy Exascale Earth System Model, *J. Adv. Model Earth Sy.*,
578 11, 2377–2411, <https://doi.org/10.1029/2019MS001629>, 2019.

579 Seinfeld, J. H., Carmichael, G. R., Arimoto, R., Conant, W. C., Brechtel, F. J., Bates, T.
580 S., Cahill, T. A., Clarke, A. D., Doherty, S. J., Flatau, P. J., Huebert, B. J., Kim, J.,
581 Markowicz, K. M., Quinn, P. K., Russell, L. M., Russell, P. B., Shimizu, A.,
582 Shinozuka, Y., Song, C. H., Tang, Y., Uno, I., Vogelmann, A. M., Weber, R. J., Woo,
583 J.-H., and Zhang, X. Y.: ACE-ASIA: Regional Climatic and Atmospheric
584 Chemical Effects of Asian Dust and Pollution, *Bull. Am. Meteorol. Soc.*, 85, 367–
585 380, <https://doi.org/10.1175/BAMS-85-3-367>, 2004.

586 Shi, L., Zhang, J., Yao, F., Zhang, D., and Guo, H.: Drivers to dust emissions over dust
587 belt from 1980 to 2018 and their variation in two global warming phases, *Sci. Total*
588 *Environ.*, 767, 144806, <https://doi.org/10.1016/j.scitotenv.2020.144860>, 2021.

589 Sivakumar M. V.: Impacts of Sand Storms/Dust Storms on Agriculture, in: *Natural*
590 *Disasters and Extreme Events in Agriculture*, edited by: Sivakumar M.V., Motha
591 R.P., and Das H.P. Springer, Berlin, Heidelberg, 159–177,
592 https://doi.org/10.1007/3-540-28307-2_10, 2005.

593 Trenberth K. E.: The definition of El Niño, *Bull. Am. Meteorol. Soc.*, 78(12), 2771–
594 2778, [https://doi.org/10.1175/1520-0477\(1997\)078<2771:TDOENO>2.0.CO;2](https://doi.org/10.1175/1520-0477(1997)078<2771:TDOENO>2.0.CO;2),
595 1997.

596 Wang, H., Easter, R. C., Zhang, R., Ma, P.-L., Singh, B., Zhang, K., Ganguly, D., Rasch,
597 P. J., Burrows, S. M., Ghan, S. J., Lou, S., Qian, Y., Yang, Y., Feng, Y., Flanner,
598 M., Leung, L. R., Liu, X., Shrivastava, M., Sun, J., Tang, Q., Xie, S., and Yoon, J.-

599 H., Aerosols in the E3SM Version 1: New developments and their impacts on
600 radiative forcing, *J. Adv. Model. Earth Sys.*, 12, e2019MS001851,
601 <https://doi.org/10.1029/2019MS001851>, 2020.

602 [Wang, S., Yu, Y., Zhang, X., Lu, H., Zhang, X., and Xu, Z.: Weakened dust activity over](#)
603 [China and Mongolia from 2001 to 2020 associated with climate change and land-](#)
604 [use management, *Environ. Res. Lett.*, 16, 124056, \[https://doi.org/10.1088/1748-\]\(https://doi.org/10.1088/1748-9326/ac3b79\)](#)
605 [9326/ac3b79](#), 2021.

606 Wu, M., Liu, X., Yang, K., Luo, T., Wang, Z., Wu, C., Zhang, K., Yu, H., and Darmenov,
607 A.: Modeling Dust in East Asia by CESM and Sources of Biases, *J. Geophys. Res.*
608 *Atmos.*, 124, 8043–8064. <https://doi.org/10.1029/2019JD030799>, 2019.

609 Wu, M., Liu, X., Yu, H., Wang, H., Shi, Y., Yang, K., Darmenov, A., Wu, C., Wang, Z.,
610 Luo, T., Feng, Y., and Ke, Z.: Understanding processes that control dust spatial
611 distributions with global climate models and satellite observations, *Atmos. Chem.*
612 *Phys.*, 20, 13835–13855, <https://doi.org/10.5194/acp-20-13835-2020>, 2020.

613 Wu, X., Okumura, Y. M., and Dinezio, P. N.: What Controls the Duration of El Niño
614 and La Niña Events?, *J. Clim.*, 32, 5941–5965, [https://doi.org/10.1175/jcli-d-18-](https://doi.org/10.1175/jcli-d-18-0681.1)
615 [0681.1](https://doi.org/10.1175/jcli-d-18-0681.1), 2019.

616 Xia, W., Wang, Y., Chen, S., Huang, J., Wang, B., Zhang, G. J., Zhang, Y., Liu, X., Ma,
617 J., Gong, P., Jiang, Y., Wu, M., Xue, J., Wei, L., and Zhang, T.: Double Trouble of
618 Air Pollution by Anthropogenic Dust, *Environ. Sci. Technol.*, 56, 761–769,
619 <https://doi.org/10.1021/acs.est.1c04779>, 2022.

620 [Xiao, D., Li, Y., Fan, S., Zhang, R., Sun, J., and Wang, Y.: Plausible influence of Atlantic](#)
621 [Ocean SST anomalies on winter haze in China, *Theor. Appl. Climatol.*, 122, 249-](#)
622 [257, <https://doi.org/10.1007/s00704-014-1297-6>, 2015.](#)

623 Yang, Y., Russell, L. M., Xu, L., Lou, S., Lamjiri, M. A., Somerville, R. C. J., Miller,
624 A. J., Cayan, D. R., DeFlorio, M. J., Ghan, S. J., Liu, Y., Singh, B., Wang, H., Yoon,
625 J.-H., and Rasch, P. J.: Impacts of ENSO events on cloud radiative effects in
626 preindustrial conditions: Changes in cloud fraction and their dependence on
627 interactive aerosol emissions and concentrations, *J. Geophys. Res. Atmos.*, 121,
628 6321–6335, <https://doi.org/10.1002/2015jd024503>, 2016a.

629 Yang, Y., Russell, L. M., Lou, S., Liu, Y., Singh, B., and Ghan, S. J.: Rain-aerosol
630 relationships influenced by wind speed, *Geophys. Res. Lett.*, 43, 2267–2274,
631 <https://doi.org/10.1002/2016GL067770>, 2016b.

632 Yang, Y., Russell, L. M., Lou, S., Liao, H., Guo, J., Liu, Y., Singh, B., and Ghan, S. J.:

633 Dust-wind interactions can intensify aerosol pollution over eastern China, *Nat.*
634 *Commun.*, 8, 15333, <https://doi.org/10.1038/ncomms15333>, 2017.

635 Yin, Z., Wan, Y., Zhang, Y., and Wang, H.: Why super sandstorm 2021 in North China?,
636 *Natl. Sci. Rev.*, <https://doi.org/10.1093/nsr/nwab165>, 2021.

637 Yu, X., Wang, Z., Zhang, H., and Zhao, S.: Impacts of different types and intensities of
638 El Nino events on winter aerosols over China, *Sci. Total Environ.*, 655, 766–780,
639 <https://doi.org/10.1016/j.scitotenv.2018.11.090>, 2019.

640 Yu, Y. and Ginoux, P.: Assessing the contribution of the ENSO and MJO to Australian
641 dust activity based on satellite- and ground-based observations, *Atmos. Chem.*
642 *Phys.*, 21, 8511–8530, <https://doi.org/10.5194/acp-21-8511-2021>, 2021.

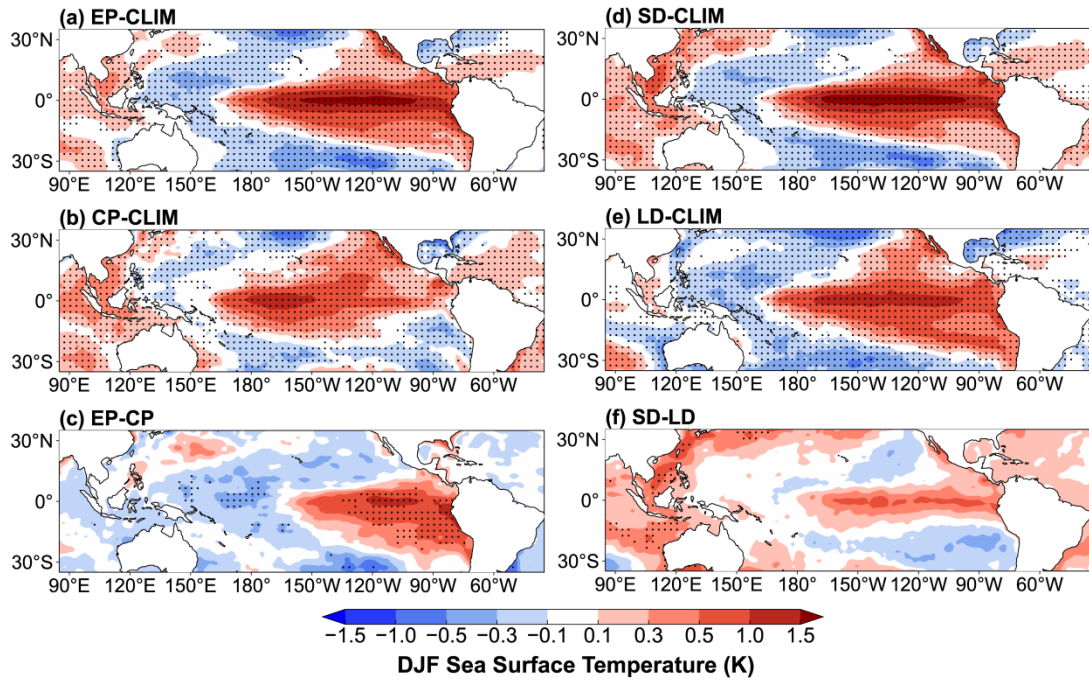
643 Zender, C. S., Bian, H., and Newman, D.: Mineral Dust Entrainment and Deposition
644 (DEAD) model: Description and 1990s dust climatology, *J. Geophys. Res.*, 108,
645 4416, <https://doi.org/10.1029/2002JD002775>, 2003.

646 Zeng, L., Yang, Y., Wang, H., Wang, J., Li, J., Ren, L., Li, H., Zhou, Y., Wang, P., and
647 Liao, H.: Intensified modulation of winter aerosol pollution in China by El Niño
648 with short duration, *Atmos. Chem. Phys.*, 21, 10745–10761,
649 <https://doi.org/10.5194/acp-21-10745-2021>, 2021.

650 Zhao, S., Zhang, H., and Xie, B.: The effects of El Niño-Southern Oscillation on the
651 winter haze pollution of China, *Atmos. Chem. and Phys.*, 18, 1863–1877,
652 <https://doi.org/10.5194/acp-18-1863-2018>, 2018.

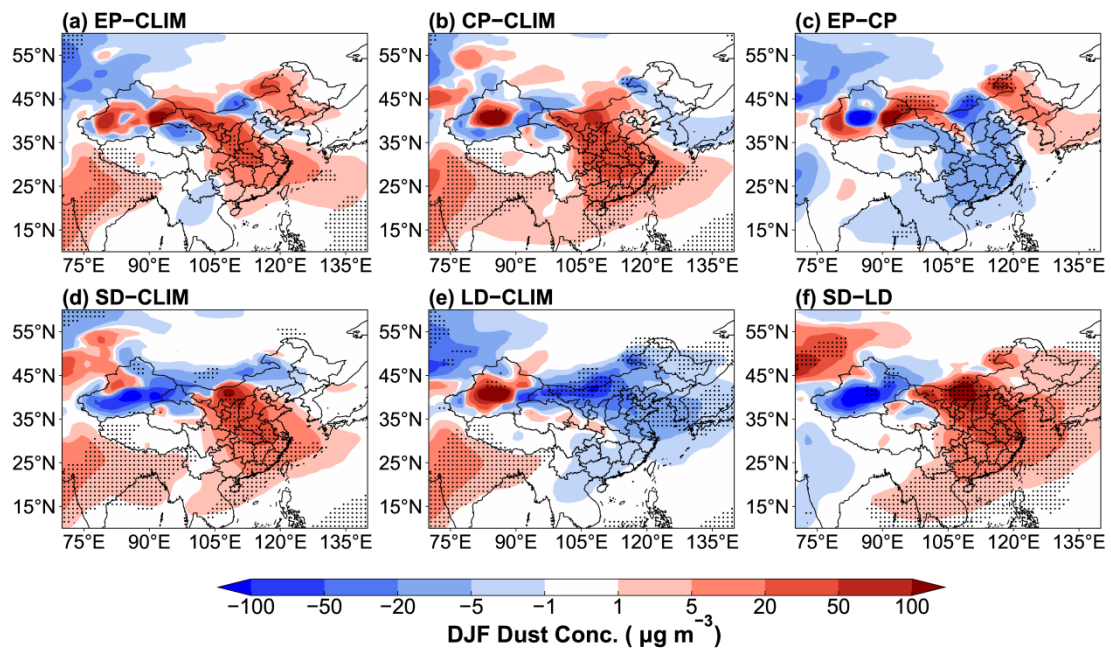
653 Zhu, C., Wang, B., and Qian, W.: Why do dust storms decrease in northern China
654 concurrently with the recent global warming?, *Geophys. Res. Lett.*, 35, L18702,
655 <https://doi.org/10.1029/2008GL034886>, 2008.

656



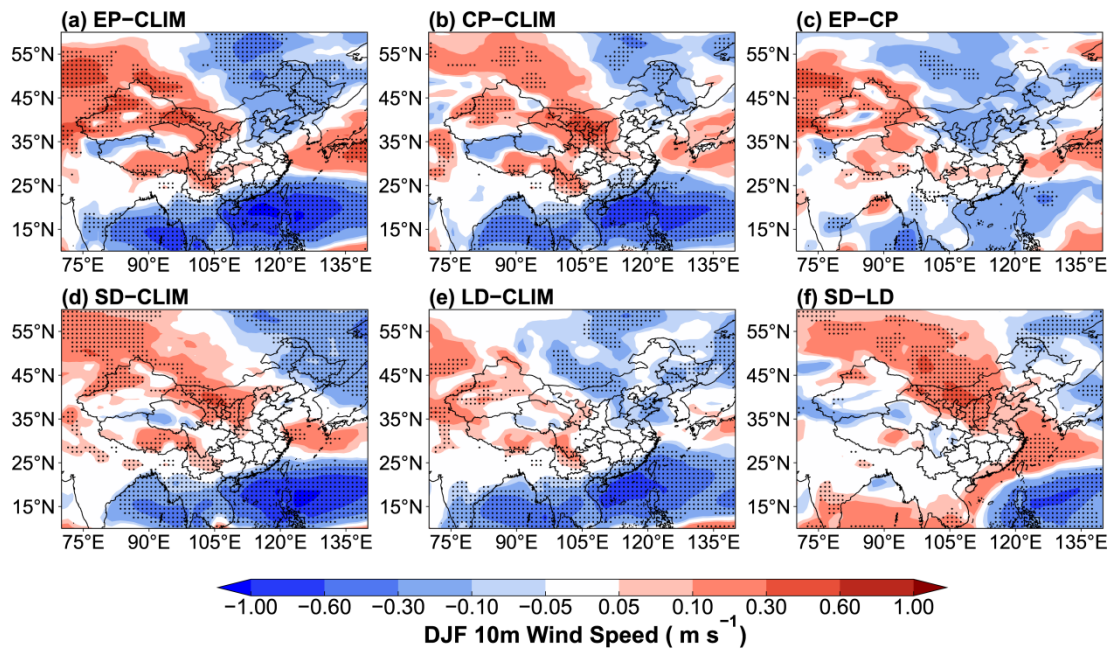
657
 658
 659
 660
 661
 662

Figure 1. Composite differences in DJF mean SST ($^{\circ}\text{C}$) between (a) EP, (b) CP, (d) SD, (e) LD El Niño events and climatological mean over 1870–2017, and (c) between EP and CP, and (f) between SD and LD El Niño events. Statistically significant differences at 98.99% from a two-tailed T-test are stippled.



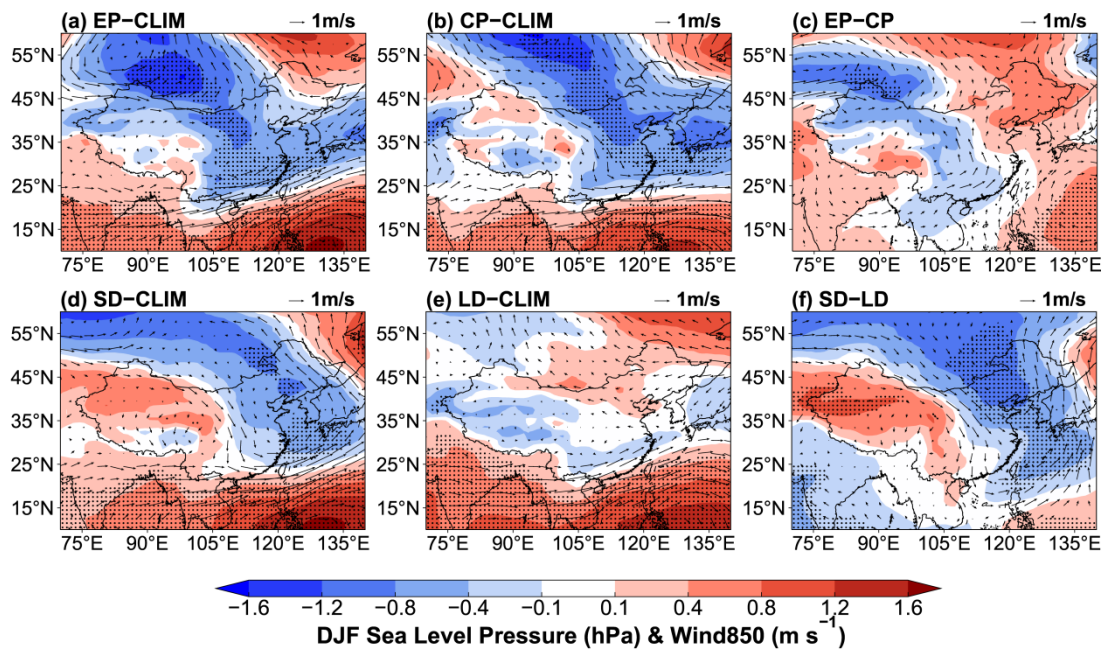
663
 664
 665
 666
 667
 668

Figure 2. Composite differences in DJF mean near-surface dust concentrations ($\mu\text{g m}^{-3}$) between EP and CLIM in (a), CP and CLIM in (b), EP and CP in (c), SD and CLIM in (d), LD and CLIM in (e), and SD and LD in (f). The stippled areas indicate statistical significance with 90% confidence from a two-tailed T-test.



669
 670
 671
 672
 673
 674

Figure 3. Composite differences in DJF mean 10-m wind speed (m s^{-1}) between EP and CLIM in (a), CP and CLIM in (b), EP and CP in (c), SD and CLIM in (d), LD and CLIM in (e), and SD and LD in (f). The stippled areas indicate statistical significance with 90% confidence from a two-tailed T-test.

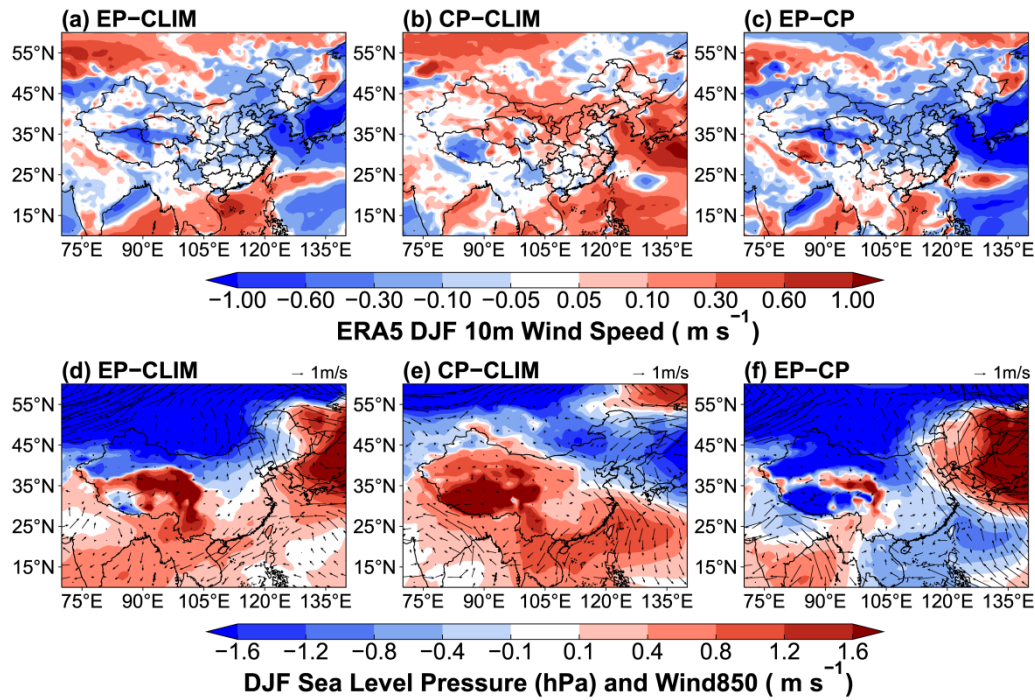


676

677

Figure 4. Composite differences in DJF mean sea level pressure (SLP, shaded; units: hPa) and winds at 850 hPa (WIND850, vector; units: m s⁻¹) between EP and CLIM in (a), CP and CLIM in (b), and EP and CP in (c), SD and CLIM in (d), LD and CLIM in (e), and SD and LD in (f). The stippled areas indicate statistical significance with 90% confidence from a two-tailed T-test.

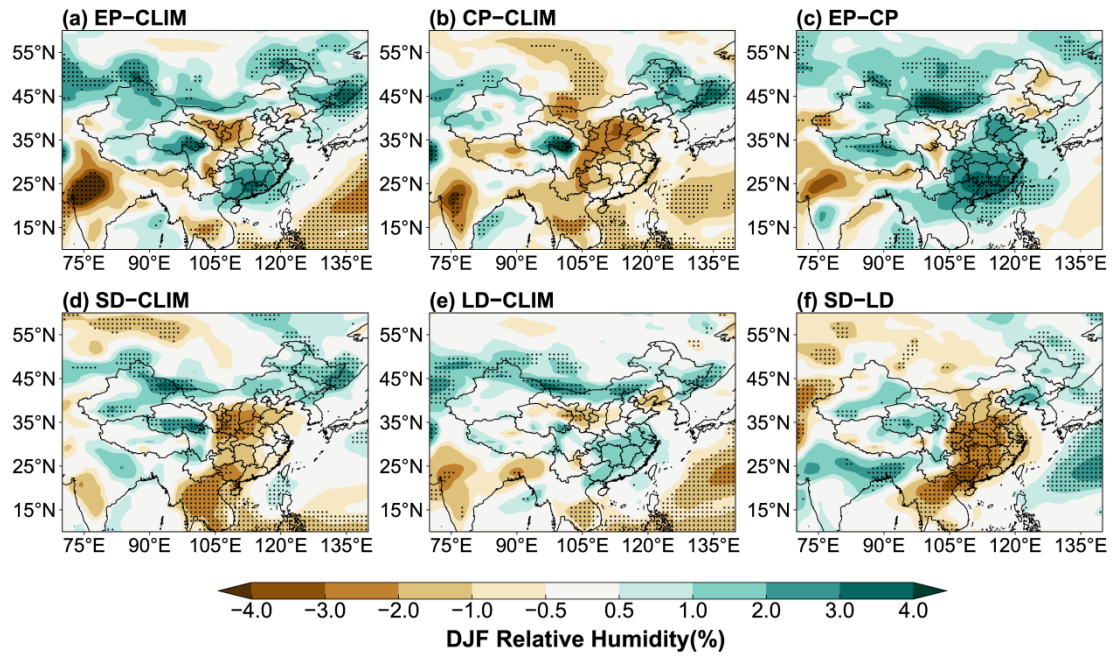
681



682

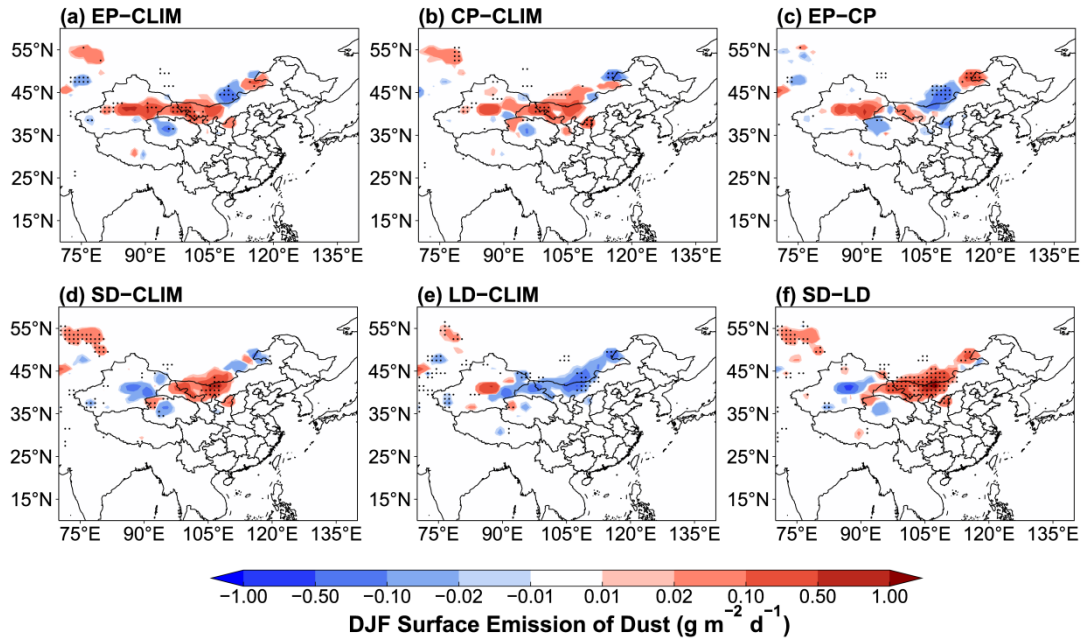
683 **Figure 5.** Composite differences in DJF mean 10-m wind speed (m s^{-1}) (top panels) and [sea level](#)
 684 [pressure \(SLP, shaded; units: hPa\) and](#) wind at 850 hPa ([WIND850](#), vector; units: m s^{-1}) (bottom
 685 panels) between 2006/07 EP El Niño and climatological mean (1950–2017) in (a, d), 2014/15 CP
 686 El Niño and climatological mean in (b, e), and 2006/07 EP El Niño and 2014/15 CP El Niño in (c,
 687 f) from the ERA5 reanalysis data. The data were detrended over 1950–2017.

688



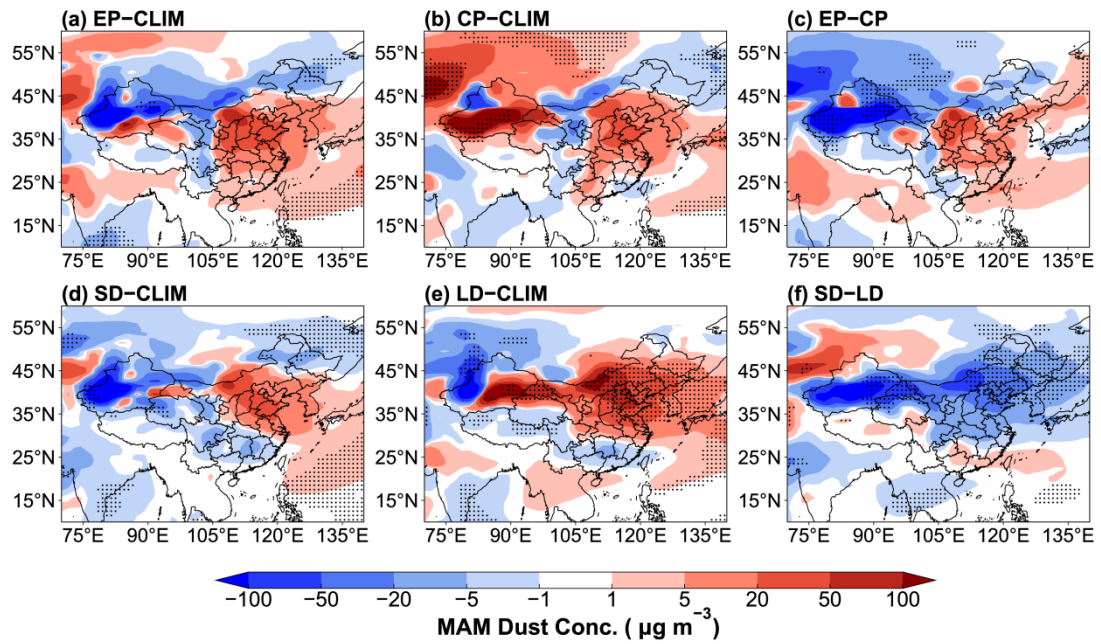
689

690 **Figure 6.** Composite differences in DJF mean relative humidity (units: %) between EP and CLIM
 691 in (a), CP and CLIM in (b), and EP and CP in (c), SD and CLIM in (d), LD and CLIM in (e), and
 692 SD and LD in (f). The stippled areas indicate statistical significance with 90% confidence from a
 693 two-tailed T-test.
 694



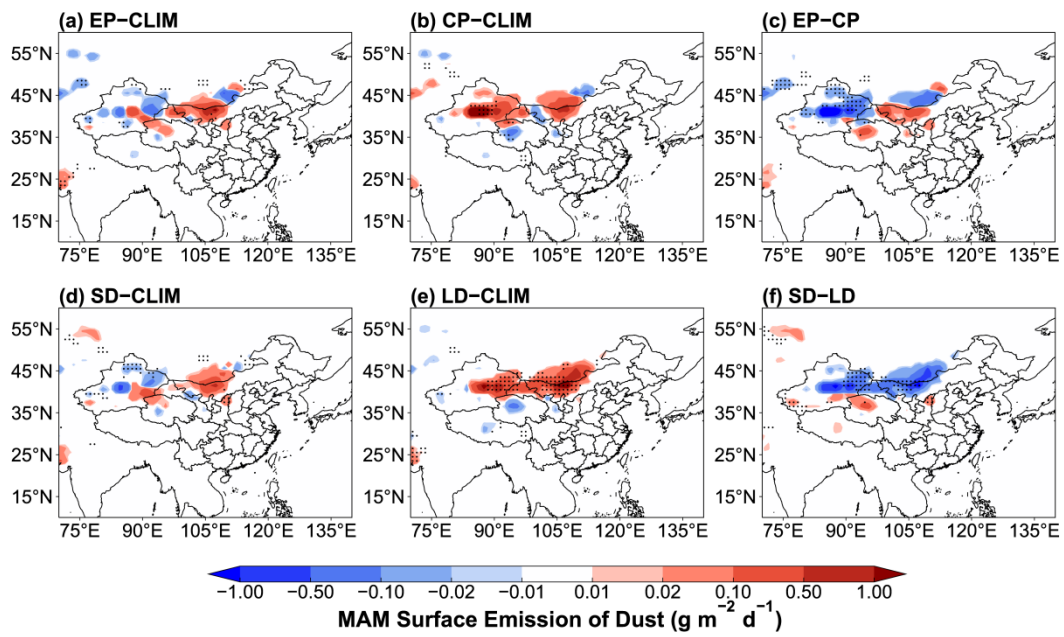
695
 696
 697
 698
 699
 700

Figure 7. Composite differences in DJF mean dust emissions ($\text{g m}^{-2} \text{d}^{-1}$) between EP and CLIM in (a), CP and CLIM in (b), EP and CP in (c), SD and CLIM in (d), LD and CLIM in (e), and SD and LD in (f). The stippled areas indicate statistical significance with 90% confidence from a two-tailed T-test.



701
 702
 703
 704
 705
 706

Figure 8. Composite differences in MAM mean near-surface dust concentrations ($\mu\text{g m}^{-3}$) between EP and CLIM in (a), CP and CLIM in (b), EP and CP in (c), SD and CLIM in (d), LD and CLIM in (e), and SD and LD in (f). The stippled areas indicate statistical significance with 90% confidence from a two-tailed T-test.



708

709 **Figure 9.** Composite differences in MAM mean dust emissions ($\text{g m}^{-2} \text{d}^{-1}$) between EP and CLIM
 710 in (a), CP and CLIM in (b), EP and CP in (c), SD and CLIM in (d), LD and CLIM in (e), and SD
 711 and LD in (f). The stippled areas indicate statistical significance with 90% confidence from a two-
 712 tailed T-test.
 713